Title: Quantitative Analysis of High-Resolution Microendoscopic Images for Diagnosis of Esophageal Squamous Cell Carcinoma

Short title: Microendoscopy of Esophageal Neoplasia

Authors and affiliations

Dongsuk Shin[1†], Marion-Anna Protano[2†], Alexandros D. Polydorides[3], Sanford M. Dawsey[4], Mark C. Pierce[5], Michelle Kang Kim[2], Richard A. Schwarz[1], Timothy Quang[1], Neil Parikh[2], Manoop S. Bhutani[6], Fan Zhang[7], Guiqi Wang[8], Liyan Xue[9], Xueshan Wang[7], Hong Xu[7*], Sharmila Anandasabapathy[2*], Rebecca R. Richards-Kortum[1*]

1. Department of Bioengineering, Rice University, Houston, TX

2. Division of Gastroenterology, The Mount Sinai Medical Center, New York, NY

3. Department of Pathology, The Mount Sinai Medical Center, New York, NY

4. Division of Cancer Epidemiology and Genetics, National Cancer Institute, Bethesda, MD

5. Department of Biomedical Engineering, Rutgers, The State University of New Jersey, Piscataway, NJ

6. Department of Gastroenterology, Hepatology and Nutrition, The University of Texas MD Anderson Cancer Center, Houston, TX

7. Department of Gastrointestinal Medicine, The First Hospital of Jilin University, Changchun, Jilin, China

8. Department of Endoscopy, Cancer Institute and Hospital, The Chinese Academy of Medical Sciences, Beijing, China

9. Department of Pathology, Cancer Institute and Hospital, The Chinese Academy of Medical Sciences, Beijing, China

†These authors contributed equally to the work.

* These authors contributed equally to the work and are co-corresponding authors.

Financial support: This work was supported by Grant Number R21CA156704 from the National Cancer Institute and Grant Number R01EB007594 from the National Institute of Biomedical Imaging and Bioengineering. The content is solely the responsibility of the authors and does not necessarily represent the official views of the National Cancer Institute, the National Institute of Biomedical Imaging and Bioengineering, or the National Institutes of Health.

Abbreviations: EMR, endoscopic mucosal resection; ESCN, esophageal squamous cell neoplasia; FOV, field of view; HGD, high-grade dysplasia; HRME, high-resolution microendoscope; HD-WLE, high-definition white light upper endoscopy; IND, Investigational New Drug; LCE, Lugol's chromoendoscopy; LGD, low-grade dysplasia; N/C ratio, nuclear-to-cytoplasmic area ratio; QC, quality control; RFA, radiofrequency ablation; ROC, receiver operating characteristic; ROI, region of interest.

Corresponding author: Rebecca R. Richards-Kortum, Rice University, 6100 Main Street, Houston, TX 77005. Phone: 713-348-3823; Fax: 713-348-5877; E-mail: rkortum@rice.edu

Potential competing interests: Rebecca R. Richards-Kortum serves as an unpaid scientific advisor to Remicalm LLC, holds patents related to optical diagnostic technologies that have been licensed to Remicalm LLC, and holds minority ownership in Remicalm LLC.

Specific author contribution: DS, MP conducted experiments, performed analyses and wrote the manuscript. AP, SD, MCP, MK, RS, TQ, NP, MB, FZ, GW, LX and XW

conducted experiments and performed analysis. HX, SA and RRK planned the project, designed and conducted experiments, wrote the manuscript, and supervised the entire project.

Abstract

Background & Aims: High-resolution microendoscopy is an optical imaging technique with the potential to improve the accuracy of endoscopic screening for esophageal squamous neoplasia. Although these microscopic images can readily be interpreted by trained personnel, quantitative image analysis software could facilitate the use of this technology in low-resource settings. In this study we developed and evaluated quantitative image analysis criteria for the evaluation of neoplastic and non-neoplastic squamous esophageal mucosa.

Methods: We performed image analysis of 177 patients undergoing standard upper endoscopy for screening or surveillance of esophageal squamous neoplasia, using high-resolution microendoscopy, at 2 hospitals in China and 1 in the United States from May 2010 to October 2012. Biopsies were collected from imaged sites (n=375); a consensus diagnosis was provided by 2 expert gastrointestinal pathologists and used as the standard.

Results: Quantitative information from the high-resolution images was used to develop an algorithm to identify high-grade squamous dysplasia or invasive squamous cell cancer, based on histopathology findings. Optimal performance was obtained using mean nuclear area as the basis for classification, resulting in sensitivities and specificities of 93% and 92% in the training set, 87% and 97% in the test set, and 84% and 95% in an independent validation set, respectively.

Conclusions: High-resolution microendoscopy with quantitative image analysis can aid in the identification of esophageal squamous neoplasia. Use of software-based image guides may overcome issues of training and expertise in low-resource settings, allowing for widespread use of these optical biopsy technologies.

Keywords: esophageal cancer; HRME; quantitative diagnosis; diagnostic.

Introduction

There is an urgent global need to improve early diagnosis of esophageal squamous cell neoplasia (ESCN).[1,2] The five-year survival rate of ESCN in the United States is only 19%, primarily because diagnosis is often at an advanced, incurable stage.[3] In low-resource settings, the five-year survival is much lower; for example, in Golestan Province, Iran, it is 3.4%.[4] At present, the current standard of care for endoscopic screening is Lugol's chromoendoscopy (LCE) with targeted biopsy of areas that do not retain dye.[5] The sensitivity of LCE is >95%, but specificity is poor (<65%).[6,7] Areas of inflammation often appear indistinguishable from superficially invasive carcinoma, leading to high false positive rates. Confocal microendoscopy, a high-resolution imaging technique, has revolutionized endoscopic surveillance for neoplasia by allowing detection at the subcellular level.[8] When confocal imaging is paired with LCE, accuracy rates have been shown to approach 95% with dramatic improvement in specificity.[9] However, existing platforms are expensive ($150,000-$300,000) and available only in a handful of tertiary centers.

Thus, there remains an essential need for easily accessible, complementary high-resolution imaging technologies that can improve accuracy of LCE by enhancing specificity, and reducing the number of biopsies needed for accurate patient diagnosis. Ideally, low cost imaging platforms should be robust, accurate, and reproducible when used in low-resource settings where there is often a shortage of healthcare providers and frequent biopsies of suspected areas are not feasible because of the scarcity and high cost of pathology services. We recently developed a fiber-optic high-resolution microendoscope (HRME) that provides images of the surface epithelium with similar

resolution to confocal endomicroscopy, but with significantly reduced system complexity and cost.[10] The cost-of-goods to assemble an HRME system is less than $3,500, including the cost of the re-usable fiber optic probe. For a detailed description of the HRME, see the Supplementary Materials. Recent studies conducted with the HRME demonstrated that sub-cellular resolution morphology can be used to detect neoplastic lesions in patients with Barrett's esophagus, breast, cervical and oral carcinoma.[11-16]

HRME images can be interpreted by trained clinical personnel at the point-of-care.[15,16] However, quantitative image analysis may provide more objective results and facilitate use of this technology in low-resource settings where trained personnel are not always available. The goal of the present study was to develop quantitative HRME image analysis criteria for delineation of neoplastic and non-neoplastic squamous esophageal mucosa.

Materials and Methods

Patients

Study participants previously scheduled to undergo screening for ESCN or surveillance for known squamous cell dysplasia underwent standard high-definition white light upper endoscopy (HD-WLE) with LCE. Written informed consent was obtained. The study was reviewed and approved by the Institutional Review Boards at The First Hospital of Jilin University (Changchun, China), The Cancer Institute at The Chinese Academy of Medical Sciences (Beijing, China), The Mount Sinai Medical Center (New York, NY), and Rice University (Houston, TX).

The endoscopist recorded the location, level, and clinical impression of each Lugol's unstained area. Lugol's unstained areas that were indeterminate or suspicious for neoplasia were further interrogated with an HRME. Prior to HRME imaging at each site, a topical solution (average 4.77 ml; range 1-10 ml) of 0.01% proflavine (P2508, Sigma-Aldrich, St. Louis, MO) in sterile phosphate buffered saline was applied to the esophageal surface using a spray catheter. Proflavine, which was used under an Investigational New Drug (IND) application from the Food and Drug Administration (IND 102 217), is a fluorescent contrast agent which stains cell nuclei. Proflavine absorbs light strongly at 445 nm, and it emits light with a peak around 510 nm. Following proflavine application, the HRME probe was inserted through the biopsy channel and the distal tip placed in gentle contact with the mucosa. Nuclei stained with proflavine were clearly visible for 5-10 minutes following application of proflavine. At each site between 1 and 113 video sequences of 1-3 seconds duration were acquired and stored as movie files so that an individual frame free of motion artifact could be

subsequently be selected for analysis. The number of video sequences collected at a given site was determined by the endoscopist's clinical judgment. The median number of video sequences collected per site was 4. HRME images were also obtained from two Lugol's stained ("normal") areas from each patient to determine the device's false negative rate. At each site imaged, the probe was used to make a superficial dimple to "mark" the imaged area for biopsy. Each imaged site was biopsied and submitted for routine histologic diagnosis. Slides were reviewed by two expert gastrointestinal pathologists (AP, SD) blinded to HD-WLE, LCE, and HRME endoscopic interpretations. Diagnosis was performed using standard criteria; samples were divided into the following categories: normal, inflammation, low-grade dysplasia (LGD), high-grade dysplasia (HGD), or cancer.[17]

Quality control and frame selection

Videos acquired with the HRME were reviewed for quality control (QC) by three observers (RRK, MP, MAP) blinded to clinical impression and pathologic diagnosis. First, one reviewer (MP) identified a single representative image frame with minimal motion artifact from each video sequence. Selected images were reviewed and those with 50% or more of the field of view (FOV) obscured by motion artifact, poor focus, or debris at the tip of the fiber bundle were excluded. At each site, a single representative image with good visual image quality was selected by reviewer consensus. In the case of a heterogeneous set of candidate images for a given site, the reviewers selected the image that appeared to correspond to the worst diagnosis.

Image analysis

Images were processed to extract features of potential use for classification (Figure 1). Images were first analyzed to exclude regions which were too dim for analysis due to uneven contact of the distal fiber tip with the epithelium, or saturated due to the presence of debris at the probe tip. Regions to be excluded were identified by applying a low-pass filter to highlight homogeneous regions of similar intensity and then thresholding to reject overly dim or saturated areas. The region of interest (ROI) was then defined as the entire field of view minus the excluded areas. Following ROI selection, Gaussian spatial filtering was applied to remove the background pattern of the HRME fiber bundle. Morphologic image processing and thresholding were used to segment nuclei. Once a threshold was determined by the histogram-based thresholding method, nuclear and cytoplasmic regions were separated by the threshold.

Following segmentation, the mean, standard deviation, and coefficient of variation of the following features were calculated for each image: nuclear size, nuclear-to-cytoplasmic area ratio (N/C ratio), nearest internuclear distance, nuclear eccentricity, nuclear solidity, and major axis of the ellipse best approximating each nucleus.

All steps shown in Figure 1 (ROI selection, filtering, segmentation, and feature calculation) are fully automated and require 3.2 seconds processing for a single image.

Image classification

Extracted features were used to develop and evaluate an algorithm to classify whether each site contained neoplastic (HGD, cancer) or non-neoplastic tissue (normal, inflammation, LGD). The decision to draw the line between LGD and HGD was consistent with confocal microendoscopic classification criteria. LGD was considered non-neoplastic as it is associated with a low rate of progression to HGD or ESCN and is

treated differently than HGD in a clinical setting. LGD is followed with serial endoscopies, while HGD can be treated with radiofrequency ablation (RFA) and/or endoscopic mucosal resection (EMR).[17,18] Data obtained at The First University Hospital and The Mount Sinai Medical Center were randomly divided into a training set to develop and optimize the algorithm, and an independent test set to estimate algorithm performance. Approximately 50% of the images were randomly assigned to the training set and 50% to the test set. Randomization was repeated until the proportion of neoplastic sites was approximately the same in the training and test sets. All images from a single patient were assigned to either the training or the test set. The data obtained at The Cancer Institute at The Chinese Academy of Medical Sciences were assigned to an independent validation set.

Two-class linear discriminant analysis was used to develop a classification algorithm. For details, see the Supplementary Materials. Image classification is fully automated and requires 0.3 seconds. Thus, the total time required to fully process and classify a single image is 3.5 seconds.

Results

Subject information – patients and sites

215 subjects were enrolled in the study; images with corresponding pathology results were available from 448 sites in 194 patients. Of these 448 sites, images from 65 sites were excluded due to QC issues (motion artifact, poor focus, or debris). Images from 8 sites were excluded because reviewers did not reach consensus on a representative image. The final data set for analysis consisted of images from 375 sites in 177 patients. Table 1 shows the histological diagnosis of measured sites in the final data set. The data obtained at The First University Hospital and The Mount Sinai Medical Center were randomly separated into training and test sets; 104 sites from 54 patients were assigned to the training set and 104 sites from 45 patients were assigned to the test set (Table 1). The remaining data obtained at The Cancer Institute at The Chinese Academy of Medical Sciences were assigned to an independent validation set which consisted of 167 sites from 78 patients (Table 1).

Table 1 Histopathologic diagnosis of measured sites and training/test/validation set composition.

	# of patients	# of sites	Histopathologic diagnosis				
			Non-neoplastic			Neoplastic	
			Normal	Inflammation	Low-Grade Dysplasia	High-Grade Dysplasia	Cancer
Training	54	104	70	13	6	8	7
Test	45	104	70	13	6	8	7
Validation	78	167	58	50	40	15	4
Total	177	375	198	76	52	31	18

Quantitative classification performance

Quantitative image features were calculated using automated image analysis. Figure 2 illustrates bar graphs of the mean quantitative image feature values for neoplastic and non-neoplastic tissue in the training set. P values were obtained with the Mann-Whitney U test. The average feature values of non-neoplastic were significantly different from those of neoplastic for all features.

A two-class linear discriminant algorithm was developed to separate neoplastic and non-neoplastic tissue using each of these features. The single best performing feature was found to be the mean nuclear area. Figure 3(a) depicts a scatter plot of this feature for each site in the training set. The decision line associated with the classifier is shown

as a straight line; the algorithm results in a sensitivity of 93% and a specificity of 92%. Figure 3(b) and 3(c) illustrate this feature for each site in the test and validation sets; the decision line developed using the training set is also shown. Applying the algorithm to the test set results in a sensitivity of 87% and a specificity of 97%, and applying it to the validation set results in a sensitivity of 84% and a specificity of 95%. Figure 4 shows the associated receiver operating characteristic (ROC) curves. The area under the ROC curve is 0.92 in the training set, 0.95 in the test set, and 0.93 in the validation set. The addition of multiple features did not improve performance.

Discussion

This study assessed the feasibility of quantitative analysis of HRME images for detection of ESCN. Using mean nuclear area, non-neoplastic and neoplastic esophageal squamous epithelium could be discriminated with a sensitivity of 87% and a specificity of 97% in the test set and 84% and 95% in the validation set compared to histopathology. For comparison, the sensitivity and specificity of LCE were 100% and 51% in the training set, 93% and 55% in the test set, and 100% and 54% in the validation set, respectively; HRME imaging is associated with substantially improved specificity relative to LCE. The use of quantitative image analysis potentially reduces the need to train endoscopists to interpret HRME images. Visual interpretation is subject to inter- and intra-observer variability which may be reduced with digital image analysis.[19] This may prove particularly useful in low-resource settings where experienced personnel are limited.

Given the limitations of existing screening approaches, the high cost of current high-resolution platforms, and the uniformly poor prognosis of invasive ECSN, there is a great need for more accurate and widely available technologies, particularly in low-resource countries with high rates of ESCN. The low specificity of endoscopic screening is a particular barrier in low-resource settings where pathology services are limited. For example, in Kenya there are approximately 40 pathologists in the country and the majority practice in Nairobi.[20] Moreover, in low-resource settings the cost of getting one biopsy processed and read is often greater than the cost of an endoscopic examination; for example, at Tenwek hospital in Kenya, these costs are $35 and $25, respectively. Thus, a robust, low-cost method of detecting squamous cell neoplasia at an early, resectable stage

with fewer biopsies could markedly improve existing endoscopic screening, surveillance and treatment. In the validation set reported here, 68 of 87 positive findings by LCE were falsely positive by histology; the improved specificity of HRME imaging could reduce the large number of false positives.

While not a commercial product, the $3,500 cost-of-goods of the HRME system suggests it could be affordable for use in low-resource settings. Over the 29 month duration of this study, five HRME systems were used without need for on-site technical support or maintenance. The HRME fiber optic probe is reusable; the only maintenance required is polishing the fiber bundle which was performed on site after the probe had been used for 60-75 procedures. The cost of proflavine was less than 1 penny per procedure. The HRME must be used in conjunction with endoscopy, but new LED-based endoscopes that reduce the cost by more than 2/3 of current systems are being introduced commercially in China.[21]

The contrast agent proflavine is an acriflavine derivative that has a long history of safe use as a topical antiseptic, and has been used for fluorescence imaging in Europe, Asia and Australia with no reports of adverse events. In our experience of >300 subjects imaged to date with proflavine, no adverse events were noted.

The strengths of this study include the fact that it was a multi-center, international, *in vivo* study with data from the first two clinical sites randomized to a training set for algorithm development and a separate test set to evaluate the performance of the algorithm relative to the standard of histopathology. In addition, performance of the algorithm was assessed in an independent validation set acquired in a different clinical setting than the training and test sets.

A limitation of this study is that image analysis was not performed in real time; instead, images were analyzed post-hoc, following acquisition. Two technical limitations currently prevent real-time analysis. (1) Quality control and frame selection are currently performed manually after the imaging session has been completed. With recent advances in automated quality control and frame selection we will now be able to perform these functions automatically within 1 minute of data collection, enabling "near real-time" analysis during the imaging session. (2) The current algorithm requires 3.5 seconds to process and classify an image, which does not permit real-time processing at 15 frames/second. Further improvements in processing speed may enable live display with automated frame-by-frame analysis.

Alternatively, the algorithm developed here could be used to enable computer assisted visual image analysis. Figure 5 shows an example of how results of the image analysis presented here can guide development of visual image interpretation guidelines to assist endoscopists in classifying HRME images. Mean nuclear area was found to be the best performing image feature, with samples classified as neoplastic if mean nuclear area exceeds 180 μm^2 (Fig. 3a); this corresponds to a mean nuclear diameter of 15.1 μm assuming circular nuclei. As a simple way to extend this approach to visual image interpretation, we added a row of 15.1 μm diameter dots to the top of each HRME image; in addition, we superimposed a grid with lines spaced 19.4 μm apart to facilitate estimation of nuclear size across the image. Observers are presented an image with the dots and grid superimposed and asked to visually assess whether most nuclei are larger than 15.1 μm in diameter; if so, then the site is diagnosed as neoplastic. The visual image interpretation guide is now embedded in the HRME imaging software and superimposed

on an image window to assist clinicians in identifying neoplastic lesions in real-time at the time of endoscopy.

In this study, a representative image for each site was selected manually by reviewer consensus. While we did not attempt to quantify the heterogeneity of images from a given site in this analysis, we note that more heterogeneity was observed in images from unstained lesions that were in fact positive by histopathology than from unstained lesions that were negative by histopathology.

While preliminary, the high accuracy and specificity of quantitative analysis of HRME images demonstrated here suggest that this technique could potentially be used to more accurately and selectively target biopsy location. The ability to analyze images quantitatively may increase utilization of such a technology, particularly in rural or community-based settings with limited access to trained clinicians. Additionally, because of improved specificity, such a technology may reduce the number of biopsies needed for accurate patient diagnosis in low-resource settings where pathology processing and reading costs are a disproportionately large component of the total cost of patient evaluation and diagnosis and there may be limited access to standard histologic analysis. Lastly, the ability to delineate normal from neoplastic mucosa in real-time, if this can be achieved, may enhance endoscopic margin detection, enabling greater accuracy for complete resection by minimally-invasive endoscopic therapies such as EMR and RFA, a less costly and less morbid alternative to surgical esophagectomy.[22] The ability of endoscopists to interpret the HRME images in real time with the assistance of the image analysis for ESCN is being studied in a prospective, international, multi-center trial.

Figures

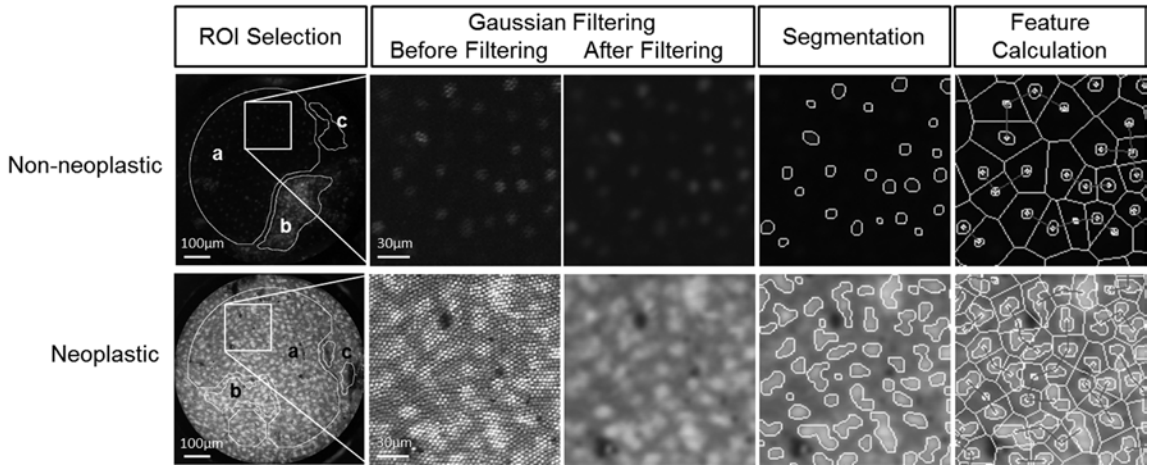

Figure 1. Quantitative image analysis process. 1) An ROI (a) is selected automatically, excluding image regions which are saturated (b) or too dim (c). 2) Fiber pattern is removed using Gaussian filtering. 3) Nuclei are segmented. 4) Quantitative image features are calculated (e.g. nearest internuclear distance).

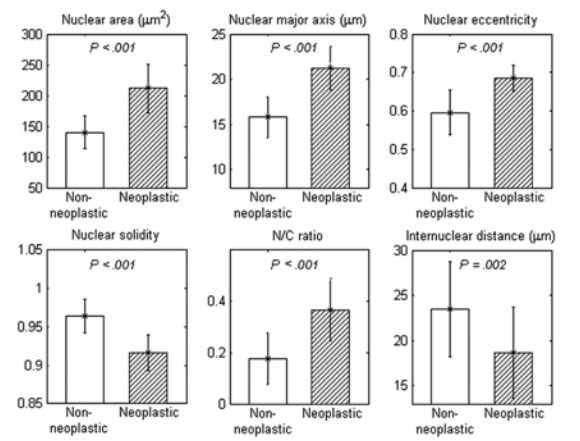

Figure 2. Bar graphs indicating mean values of six quantitative image features (± one std. dev) for non-neoplastic and neoplastic sites in the training set. P-values were obtained using the Mann-Whitney U test.

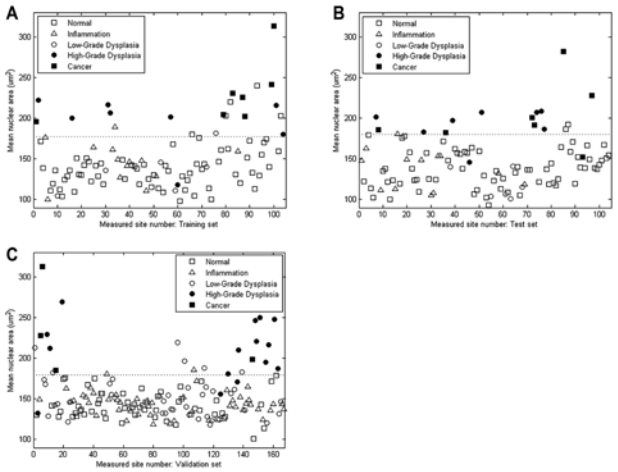

Figure 3. (a) Scatter plot of mean nuclear area for each measured site in the training set. The decision line which classifies sites as neoplastic or non-neoplastic with maximum accuracy is shown. (b) Scatter plot of mean nuclear area for each measured site in the test set. (c) Scatter plot of mean nuclear area for each measured site in the validation set. The decision line to classify sites as neoplastic or not using the training set is shown.

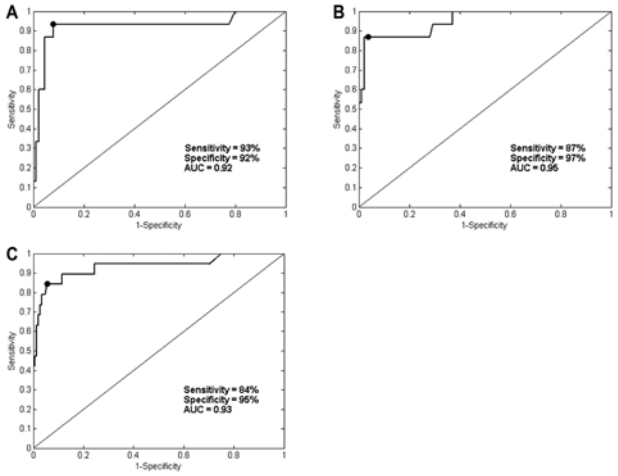

Figure 4. ROC curves for linear discriminant analysis algorithm based on the single feature of mean nuclear area applied to data in (a) the training set, (b) the test set, and (c) the validation. The Q-points correspond to a sensitivity of 93% and a specificity of 92%

in the training set (a), 87% and 97% in the test set (b), and 84% and 95% in the validation set (c).

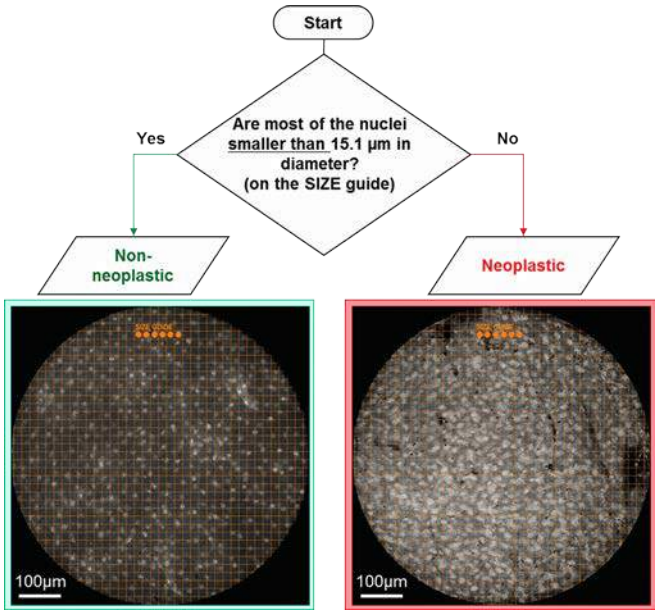

Figure 5. Flow chart illustrating visually-guided image analysis algorithm. A row of 15.1 µm diameter reference dots was added to the top of each HRME image; in addition, a grid with lines spaced 19.4 µm apart was superimposed to facilitate estimation of nuclear size across the image. Each 15.1 µm diameter reference dot occupies approximately half the area of a single square in the grid. If most nuclei appear smaller than the 15.1 µm diameter reference dots, then the image is classified as non-neoplastic; otherwise it is classified as neoplastic.

References

1. Jemal A, Bray F, Center MM et al. Global cancer statistics. CA Cancer J Clin. 2011;61(2):69–90.
2. Siegel R, Naishadham D, Jemal A. Cancer statistics, 2013. CA Cancer J Clin 2013;63(1):11-30.
3. Howlader N, Noone AM, Krapcho M et al. SEER cancer statistics review, 1975-2009 (Vintage 2009 Populations), National Cancer Institute. Bethesda, MD, http://seer.cancer.gov/csr/1975_2009_pops09/, based on November 2011 SEER data submission, posted to the SEER web site, April 2012. Accessed March 20, 2013.
4. Aghcheli K, Marjani H-A, Nasrollahzadeh D et al. Prognostic factors for esophageal squamous cell carcinoma—a population-based study in Golestan province, Iran, a high incidence area. PLoS One 2011;6(7):e22152.
5. Reddymasu SC, Sharma P. Advances in endoscopic imaging of the esophagus. Gastroenterol Clin North Am 2008;37(4):763-74.
6. Connor MJ, Sharma P. Chromoendoscopy and magnification endoscopy for diagnosing esophageal cancer and dysplasia. Thorac Surg Clin 2004;14(1):87– 94.
7. Freitag CP, Barros SG, Kruel CD et al. Esophageal dysplasias are detected by endoscopy with Lugol in patients at risk for squamous cell carcinoma in southern Brazil. Dis Esophagus 1999;12(3):191-195.
8. Iguchi Y, Niwa Y, Miyahara R et al. Pilot study on confocal endomicroscopy for determination of the depth of squamous cell esophageal cancer in vivo. J Gastroenterol Hepatol 2009;24(11):1733-1739.

9. Pech O, Rabenstein T, Manner H et al. Confocal laser endomicroscopy for in vivo diagnosis of early squamous cell carcinoma in the esophagus. Clin Gastroenterol Hepatol 2008;6(1):89-94.
10. Muldoon TJ, Pierce MC, Nida DL et al. Subcellular-resolution molecular imaging within living tissue by fiber microendoscopy. Opt Express 2007;15(25):16413–16423.
11. Muldoon TJ, Anandasabapathy S, Maru D et al. High-resolution imaging in Barrett's esophagus: a novel, low-cost endoscopic microscope. Gastrointest Endosc 2008;68(4):737–744.
12. Rosbach KJ, Shin D, Muldoon TJ et al. High-resolution fiber optic microscopy with fluorescent contrast enhancement for the identification of axillary lymph node metastases in breast cancer: a pilot study. Biomed Opt Express 2010;1(3):911-922.
13. Quinn MK, Bubi TC, Pierce MC et al. High-resolution microendoscopy for the detection of cervical neoplasia in low-resource settings. PLoS One 2012;7(9):e44924.
14. Pierce MC, Guan Y, Quinn MK et al. A pilot study of low-cost, high-resolution microendoscopy as a tool for identifying women with cervical precancer. Cancer Prev Res (Phila) 2012;5(11):1273-1279.
15. Muldoon TJ, Roblyer D, Williams MD et al. Noninvasive imaging of oral neoplasia with a high-resolution fiber-optic microendoscope. Head Neck 2012;34(3):305-312.
16. Vila PM, Park CW, Pierce MC et al. Discrimination of benign and neoplastic mucosa with a high-resolution microendoscope (HRME) in head and neck cancer. Ann Surg Oncol 2012;19:3534-3539.

17. Schlemper RJ, Riddell RH, Kato Y et al. The Vienna classification of gastrointestinal epithelial neoplasia. Gut 2000;47(2):251-255.
18. Dixon MF. Gastrointestinal epithelial neoplasia: Vienna revisited. Gut 2002; 51:130-131.
19. Downs-Kelly E, Mendelin JE, Bennett AE et al. Poor interobserver agreement in the distinction of high-grade dysplasia and adenocarcinoma in pretreatment Barrett's esophagus biopsies. Am J Gastroenterol 2008;103(9):2333–2340.
20. Adesina A, Chumba D, Nelson AM et al. Improvement of pathology in sub-Saharan Africa. Lancet Oncol 2013;14(4):e152-7.
21. Ota Y. (2014, January 24). "Olympus to sell low-cost endoscopes in China." Nikkei Asian Review. Retrieved February 10, 2014 from http://asia.nikkei.com/Tech-Science/Tech/Olympus-to-sell-low-cost-endoscopes-in-China
22. Moraca RJ, Low DE. Outcomes and health-related quality of life after esophagectomy for high-grade dysplasia and intramucosal cancer. Arch Surg 2006;141(6):545–549;discussion 549-51.

Supplementary Materials

Imaging system

The HRME system acquires fluorescence images via a coherent fiber bundle placed in contact with tissue (Supplementary Figure S1). Illumination is provided via a bandpass-filtered blue LED (FF01-452/25, Semrock, Rochester, NY; M455L2, Thorlabs, Newton, NJ). Light is reflected at a dichroic mirror (485DCLP, Chroma Technology Corp, Bellows Falls, VT) onto a 1 mm outer diameter fiber bundle (FIGH-30-850N, Fujikura, Tokyo, Japan), comprised of 30,000 optical fibers with a center-to-center spacing of 4 μm and a 720 μm field of view (FOV). Fluorescence emission returning through the bundle is imaged through the dichroic mirror and a 550 nm bandpass filter (FF03-550/88, Semrock, Rochester, NY) onto the optical sensor of a CCD camera (GRAS-14S5M, Point Grey, Richmond, Canada). The lateral and axial resolution of the system are 4.4 and 20 μm, respectively. The system is controlled by a laptop computer, which acquires and displays video at a frame rate of 15 frames per second. The endoscopic procedure using the HRME is straightforward; endoscopists who had not previously used the HRME were able to learn how to use the device within a few minutes.

Imaging classification

Two-class linear discriminant analysis was used to develop a classification algorithm using data only from the training set; image features were added one at a time until classification performance did not improve. Histologic diagnosis was considered the gold standard. The receiver operating characteristic (ROC) curve for this classifier was plotted using training set data and the optimal threshold was established at the Q-point of the ROC curve. The algorithm was then used to classify data in the test and validation

sets using this threshold. Sensitivity and specificity were calculated using histologic diagnosis as the gold standard. Finally, ROC curves were plotted for the algorithm applied to the test and validation sets.

Supplementary Figure

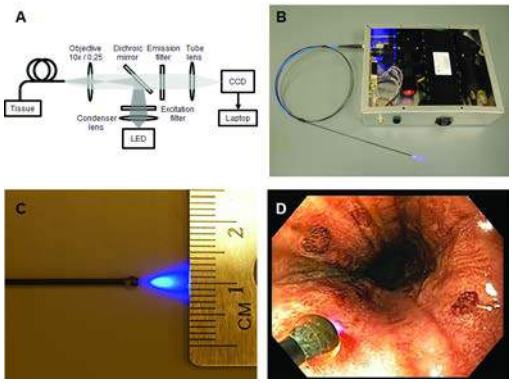

Figure S1. High Resolution Microendoscope (HRME). (a) Device configuration. Excitation light is delivered through the fiber optic bundle and the fluorescence emission from the proflavine is collected through the fiber optic bundle and focused on a CCD camera, producing images. (b) The device is battery operated and easily fits in a briefcase. (c) The probe tip is 1 mm in diameter. (d) The probe can be inserted through the operating channel of a standard endoscope and placed in gentle contact with the mucosa to obtain microendoscopic images.